ST-ECF Instrument Science Report ACS-2008-01

Updated flux calibration and fringe modelling for the ACS/WFC G800L grism

H. Kuntschner, M. Kümmel, J. R. Walsh
January 25, 2008

ABSTRACT

A revised flux calibration is presented for the G800L grism with the ACS Wide Field Channel. The calibrations were derived from observations of the HST standard star G191B2B and cross-checked with observations of the standard star GD153. The absolute flux calibration of the 1st order is accurate to better than 2% for wavelengths from 6000 to 9500 Å at the spatial positions covered in this ISR. The updated flux calibration file shows differences of less than 5% to the previous one and is made available to users as configuration files for the aXe software package. Furthermore, the spectral resolving power for point sources observed with the G800L grism (1st order) was measured to be 100±20 Å (FWHM) at 6563 Å. The flux calibration of other orders, which are currently not used for scientific purposes, is also updated.
In an investigation of the fringing properties of the WFC CCDs the contribution of fringing to the total error of the flux calibration is examined. Using a Gaussian model of 100 Å (FWHM) for the relative distribution of light falling onto a given CCD pixel (the so called pixel throughput function), we demonstrate that the error due to fringing amounts to less than 0.1% for continuum sources and can therefore be neglected. For narrow emission lines fringing can cause in principle line flux variations of 12% and more. For more realistic scenarios as in the case of emission lines in a Wolf Rayet star we measure variations of order 4%.

1. Introduction

The Advanced Camera for Surveys (ACS) is equipped with several dispersing elements for slitless spectroscopy. One of the most frequently used ones is the G800L grism, which can be used both with the *high resolution channel* (HRC) and with the *wide field channel* (WFC). This Instrument Science Report (ISR) describes the flux calibration for ACS/WFC G800L spectroscopy. While basic flux calibration files are already available from the ST-ECF WEB pages, this is the first ISR describing in more detail the flux calibration procedure based on archival observations of two white dwarf flux standard stars (G191B2B and GD153). Furthermore, the wavelength solution was up-dated in ISR ACS 2005-08 (Larsen & Walsh 2005) and thus a revised flux calibration based on the new wavelength scale is needed, too. The new calibration files supersede any previous ones and are applicable to all available observations.

We also include in this report an extensive investigation into the potential effects of fringing on the flux calibration based on the WFC CCDs fringing model as described in ST-ECF ISR ACS 2003-03 (Walsh et al. 2003). As part of the fringing model, a reasonably accurate estimate of the effective spectral resolving power for point sources is needed. We determine the effective spectral resolving power of the G800L grism in the WFC at the wavelength of the Hα line by broadening a model spectrum of G191B2B to match the observations.

The calibration products described here are tailored for the use with the aXe spectral reduction package (Kümmel et al. 2006) and are available to users via the aXe web page (http://www.stecf.org/instruments/ACSgrism/).

2. Data

Firstly, the HST archive was searched for suitable flux standard star observations in the WFC with the G800L grism. Observations with only partial spectral coverage or saturation problems were rejected. The final observations used in this ISR were carried out under the following programmes for G191B2B: 9568 (PI Pasquali), 10374 (PI Giavalisco) and for GD153: 9029 (PI Pasquali). All data were downloaded from the ST-ECF archive with a standard on-the-fly pipeline processing.

As shown in Figures 1 and 2, the observations cover various spatial positions on both chips of the WFC. In total there are eleven different positions for G191B2B and two spatial positions for GD153 (the position at x=3250 and y=630 on chip 2 actually consists of two separate observations shifted by approximately one pixel). For each position, a combination of direct and grism images was observed. For some of the observations only sub-arrays were read out in order to minimize

overheads. A list of the individual files used in this report is given in Appendix A along with auxiliary information such as exposure time, spatial pointing etc.

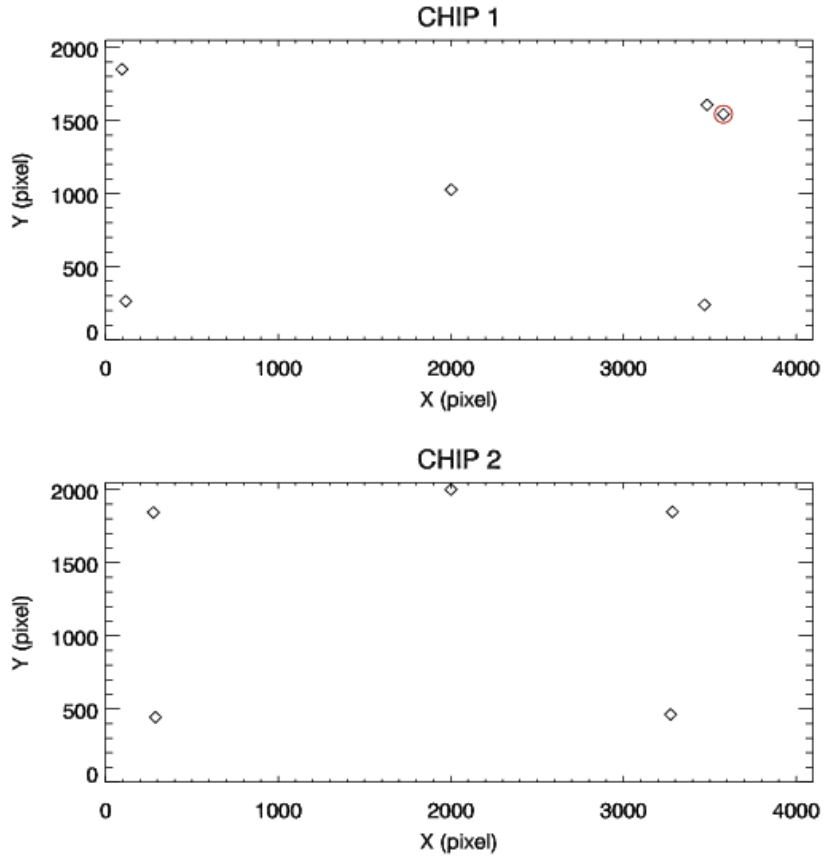

Figure 1: Map of the spatial positions for standard star G191B2B from proposal 9568. The only observation from proposal 10374 is marked with a red circle.

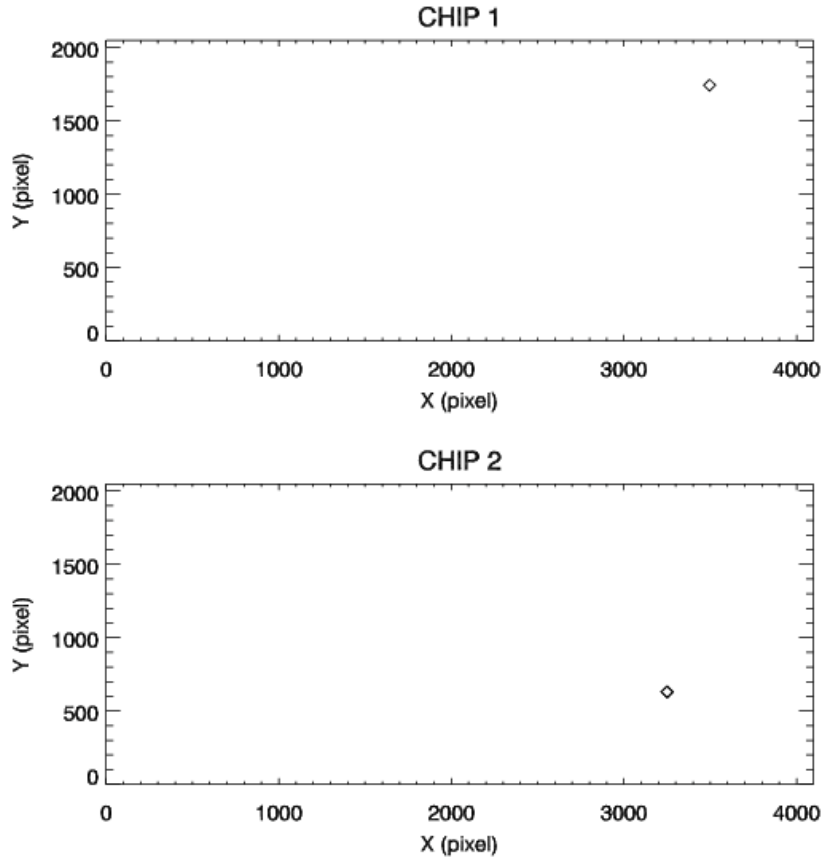

Figure 2: Map of spatial positions for standard star GD153 from proposal 9029. The position at x=3250 and y=630 on chip 2 consists of two separate observations shifted by approximately one pixel.

3. Initial data processing and extraction of spectra

Following standard on-the-fly archive pipeline processing, the readouts of sub-arrays were copied into full ACS/WFC sized images. Thereafter, observations of a given standard star at the same spatial position were combined with the IRAF routine imcombine using cosmic ray rejection. All the following reduction steps were carried out with the aXe reduction package. The extraction was performed with an extraction aperture of ±10 pixels for a total height of 20 pixels (corresponding to ±0.5 arcsec) and the local background was determined in 70 pixel wide bands at a distance of more than 85 pixels above and below the spectrum. Due to the sub-array readouts there was not always a full 70 pixels of background available.

4. Flux calibration

The extracted spectra of the white dwarf standard star G191B2B (first order; in units of electrons per pixel per sec) were converted to units of electrons per Å per sec and divided by a smoothed (100 Å FWHM; see also Section 6) version of the model spectrum taken from the HST CALSPEC library (g191b2b_mod_004.fits). At each wavelength bin, the median of all the individual sensitivity curves was taken to produce a combined sensitivity function and applying a robust smoothing in a sliding 12 pixels window to derive the final sensitivity function. The error is evaluated by taking the standard deviation of all individual sensitivity curves at each wavelength bin and imposing a minimum error of 1%.

Using this new sensitivity curve, Figure 3 shows (from the top) the aXe-extracted spectra in electrons per second per pixel, in flux units and the ratio of the observed flux over the model spectrum versus wavelength.

In the top plot of Figure 3, significant variations between spectra can be seen since the spectral dispersion (Å/pixel) changes as a function of position within the field-of-view. The overall agreement between the fully calibrated standard star spectra (middle plot) is excellent for the wavelength range 6000 to 9500 Å, with a standard deviation of 0.9%. However, for wavelength shortwards of 6000 Å and redwards of 9500 Å there is a marked increase in fluctuations reaching levels of 10% at about 5500 Å and approximately 5% at 10000 Å. The rather large error in flux calibration at short wavelength is explained by a sharp drop in the total transmission of the instrument (see also Figure 6) where small wavelength calibration errors produce large variations in measured flux. We note a possible 2^{nd} order contamination for wavelength greater than about 10000 Å which may affect the flux calibration of the 1^{st} order.

There are also systematic trends visible in Figure 3 (bottom panel), indicating that between 7000 and 9500 Å aXe extracted and calibrated observations located on CHIP 2 seem to have too much flux (at the 1% level) and vice versa for CHIP 1. Most probably these systematic differences are caused by an imperfect, wavelength dependent large-scale flat-field correction. The currently available observations are not sufficient to robustly improve the large-scale flat-field and thus we decided to keep the current calibration.

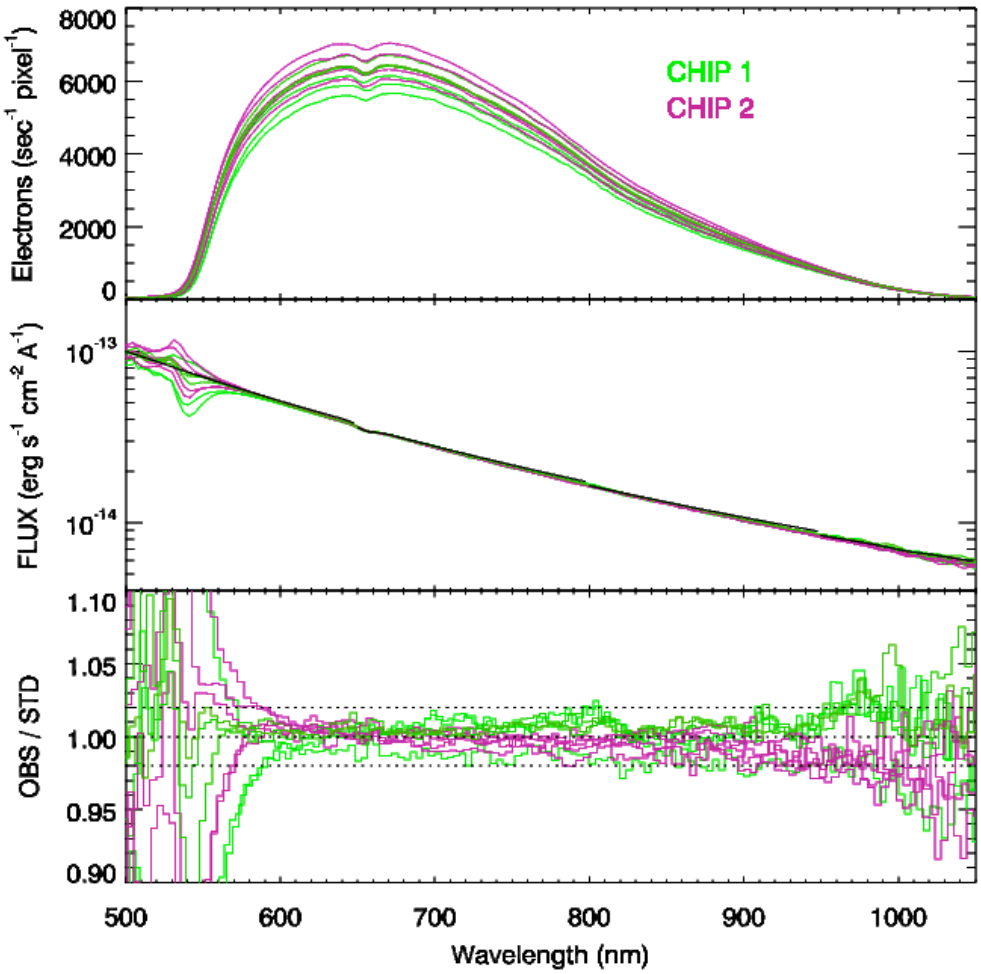

Figure 3: The aXe extracted 1-dimensional spectra of the standard star G191B2B in units of electrons per second per pixel, fully calibrated flux units and the ratio of the observed flux over the model spectrum versus wavelength (from top to bottom). Observations obtained on different CCDs are color-coded as indicated in the upper panel.

As an independent check of our revised flux calibration we have extracted spectra of the HST flux standard star GD153 with the aXe software and the newly derived sensitivity curve (see Figure 4). There are three independent exposures, one on CHIP 1 and two on CHIP 2 (see also Figure 2). We find similar systematic trends with wavelength as for the star G191B2B (see Figure 3). Overall we conclude that our absolute flux calibration for the first order spectra is better than 2% for wavelength between 6000 and 9500 Å and for the spatial positions covered in this ISR.

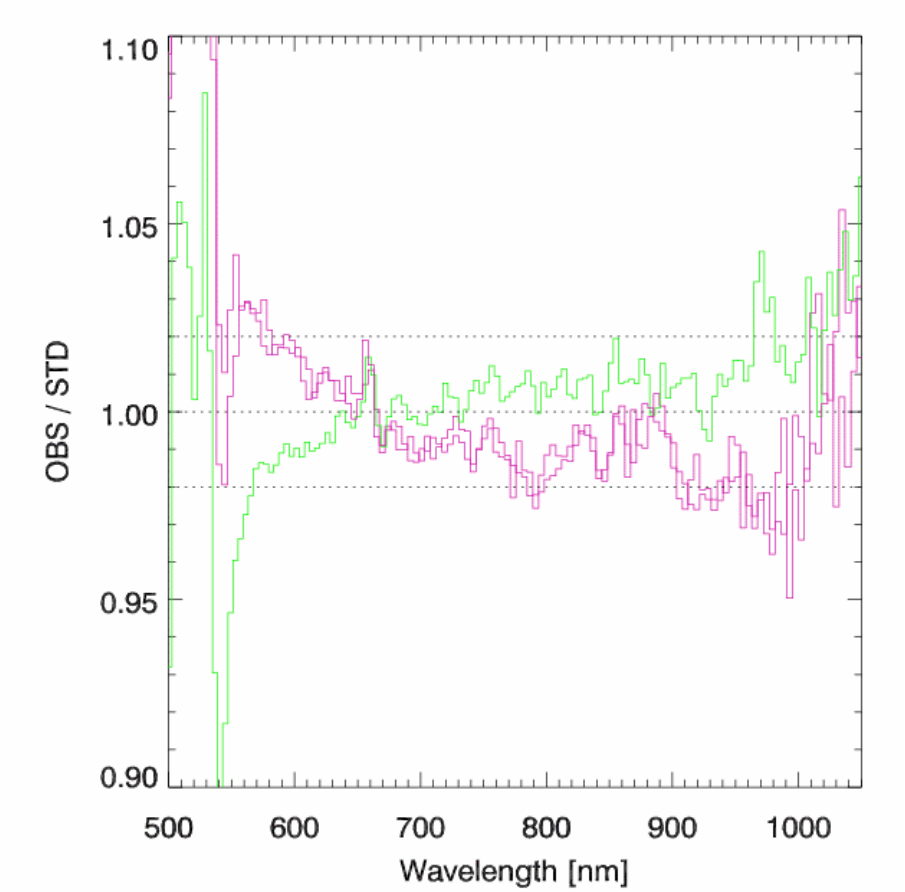

Figure 4: The aXe extracted spectra of the standard star GD153, shown as the ratio of the observed flux over the model spectrum versus wavelength. Observations obtained on different CCDs are color-coded, as indicated in Figure 3.

From the sensitivity curves it is straightforward to calculate the total system throughput of the ACS/WFC G800L spectroscopy mode, shown in Figure 5. For the 1st order the throughput peaks at 34.5% for wavelength around 7300 Å. For wavelength shorter than about 5600 Å there is a sharp drop in total system throughput caused by the declining grism efficiency.

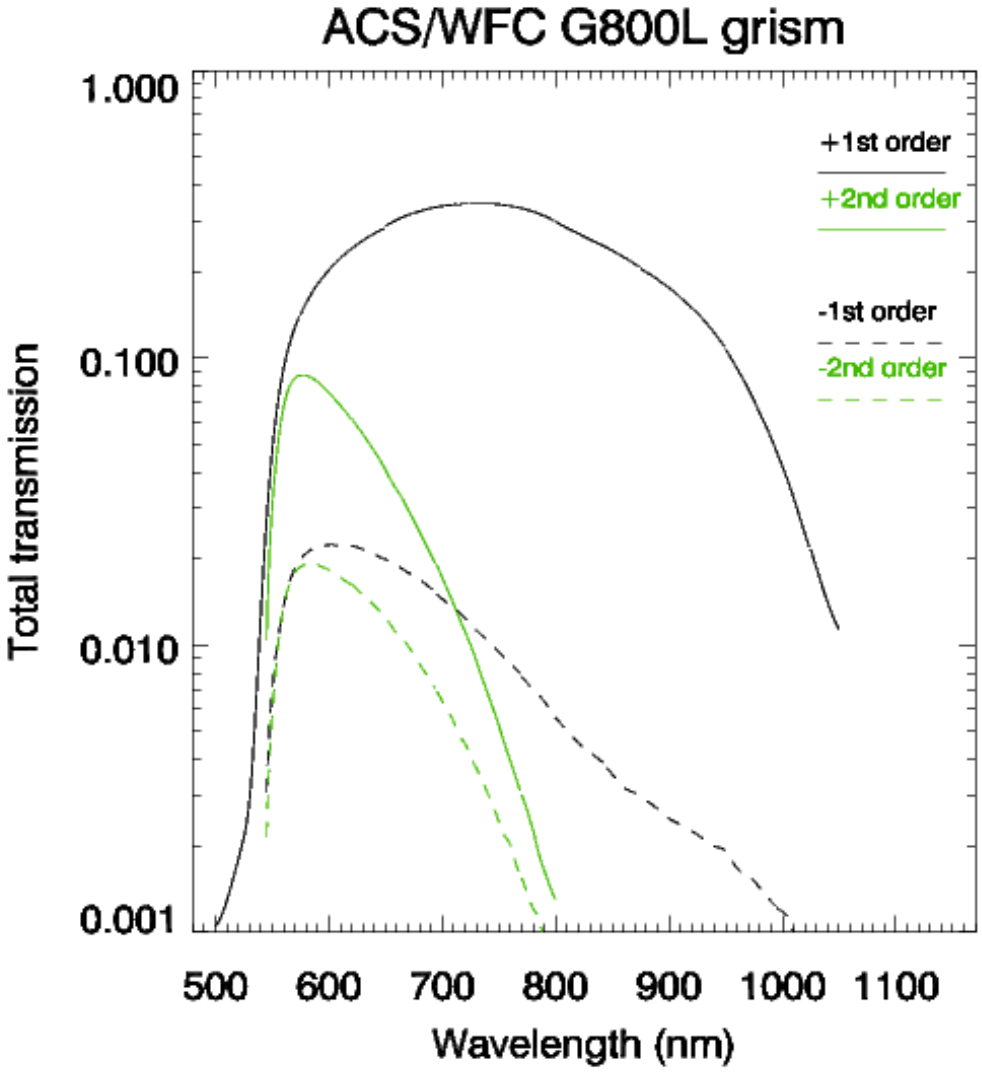

Figure 5: Total throughput of the +1st, +2nd, -1st, and -2nd orders of the G800L grism in the WFC, derived from the sensitivity curves of this report.

In Figure 6 we compare our newly derived sensitivity curve with the one used up to now (ACS.WFC.1st.sens.6.fits) in the aXe software package. Apart from edge effects there are only moderate differences with a maximum of 5%. Overall there is a roughly linear gradient in sensitivity differences such that the revised curve predicts less sensitivity in the blue. The differences are largely explained by a revised wavelength calibration that was published in ST-ECF ISR ACS 2005-08 (Larsen & Walsh 2005) and not available for the original sensitivity files.

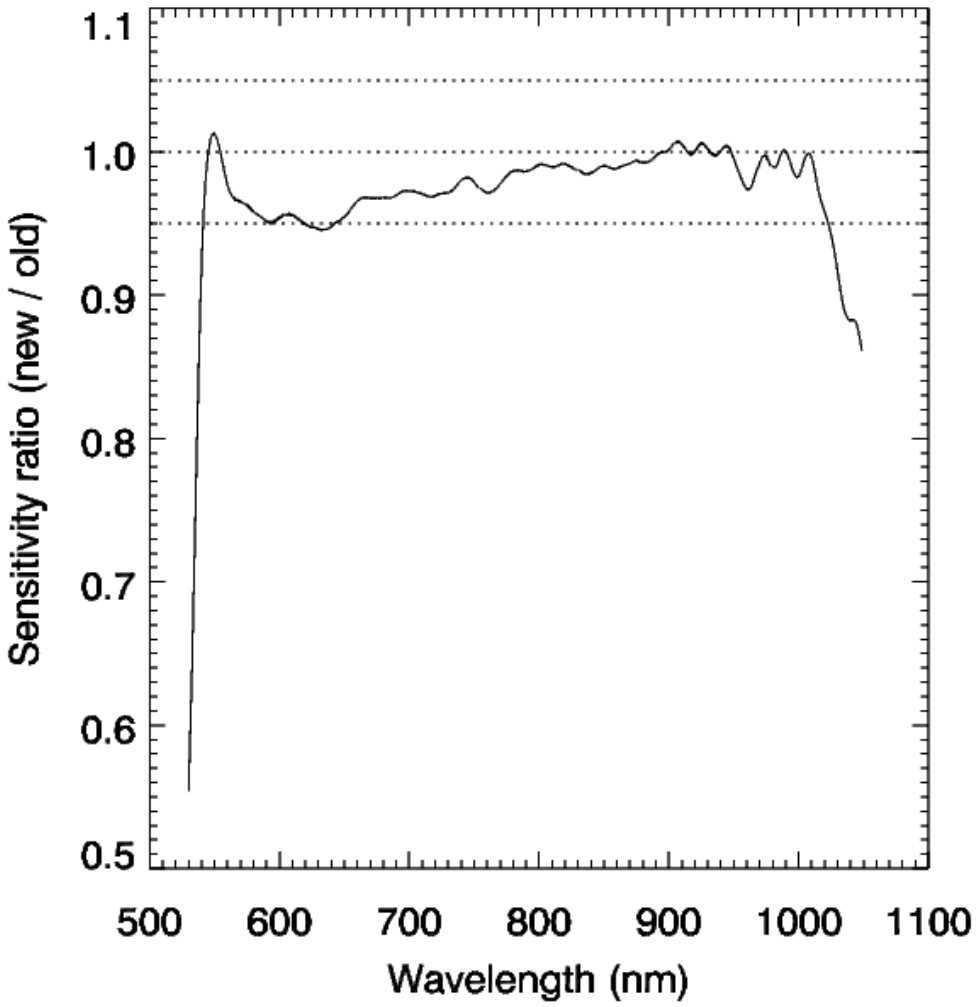

Figure 6: Comparison of old and new sensitivity curves. The dotted lines indicate the 0.95, 1.00, and 1.05 levels.

The above mentioned report focused only on the (positive) first order of the G800L grism. Following the same procedure we also updated the sensitivity files of the other orders (-3 ... +3), which are typically not used for scientific purposes, but can be of use for contamination calculations. The overall flux calibration for the other orders is reasonable, with standard deviations of up to 10% between different exposures of the same star. Note, that we do not always have the full set of 11 exposures of G191B2B available since parts of the spectrum are located outside the detector area. There also remain systematic differences between CHIP1 and CHIP2; this is particularly visible for the second, positive order. The total system throughput for the positive and negative first and second orders is summarized in Figure 5.

We note, that what we call 3rd order and treat technically as one order, is actually the superposition of the 3rd and higher orders of the grism. Technically this solution produces good results for contamination calculations, but scientifically the wavelength and flux calibration is wrong in the overlapping regions and thus the spectra of the "3rd" order should not be used for scientific purposes. Independent wavelength solutions have only been established up to 2nd order but not for higher orders.

A summary of all updated sensitivity files is given in Table 1 and also available from the ACS WEB pages at the ST-ECF:

http://www.stecf.org/instruments/ACSgrism

Table 1: List of sensitivity files, which were re-derived and updated as part of this report.

Spectral order	Sensitivity file derived in this report
+1	ACS.WFC.1st.sens.7.fits
+2	ACS.WFC.2nd.sens.6.fits
+3	ACS.WFC.3rd.sens.2.fits
-1	ACS.WFC.-1st.sens.2.fits
-2	ACS.WFC.-2nd.sens.2.fits
-3	ACS.WFC.-3rd.sens.2.fits
0	ACS.WFC.0th.sens.2.fits

5. Aperture corrections

The sensitivity file produced as part of this report refers to an aperture size of ±0.5 arcsec (corresponding to ±10 pixels). For some other applications it may be desirable to use different aperture sizes. In order to quantify the loss or gain of flux for different aperture sizes, a spectrum of the flux standard G191B2B from programme 9568 was extracted for a range of aperture sizes and normalized to the flux in the default aperture. The normalized flux as a function of wavelength and aperture size at several wavelengths is shown in Figure 7. The data from Figure 7 are also listed in Table 2 in the Appendix and are available from the aXe WEB pages in electronic form (http://www.stecf.org/instruments/ACSgrism). The corrections given here are only valid for point sources, and will typically be larger for extended objects.

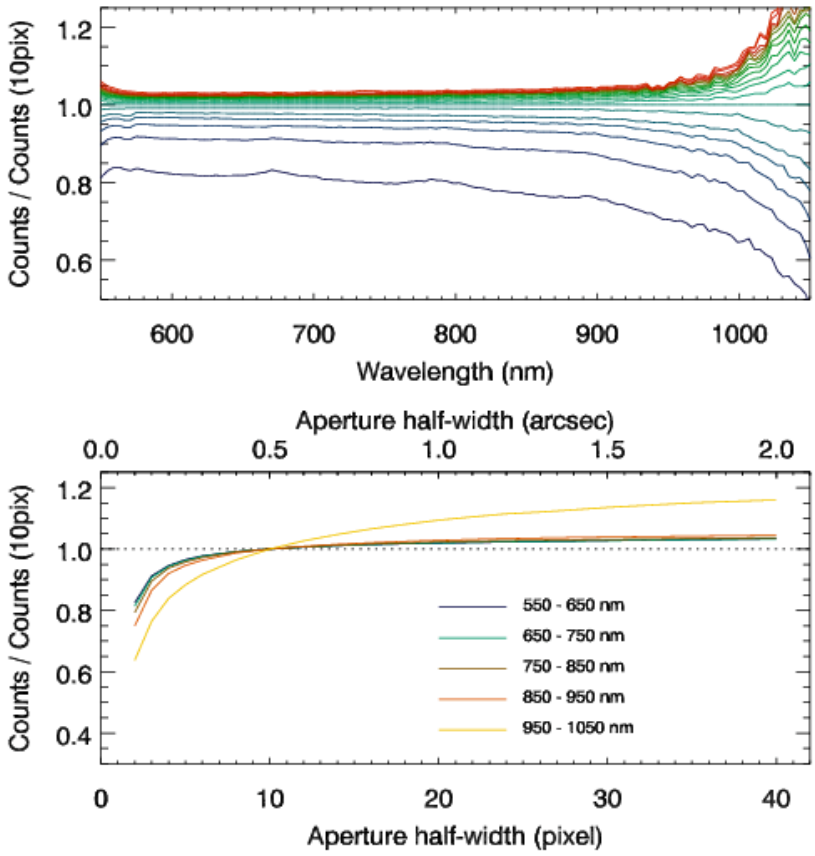

Figure 7: Normalized flux with respect to the default aperture of ±10 pixels (±0.5 arcsec) as function of wavelength and aperture half-width in pixels.

6. Effective resolving power of the G800L grism in the WFC

The nominal resolving power of the G800L grism in the 1st order is quoted as R≈100 @ 8000 Å in the Instrument Handbook. Here in this report we aim to provide an empirical measurement of the spectral resolving power by using the observations of the standard star G191B2B. The idea here is to broaden a high resolution template spectrum with a Gaussian line-spread function of varying width until it matches the observed spectrum in the region of the Hα absorption line. This test will provide an empirical measurement of the spectral resolving power at the wavelength of Hα (6563 Å). The lack of further absorption lines for white dwarf

stars in the spectral range covered by the G800L grism prohibits deriving the resolving power as function of wavelength[1].

Before we describe our measurements we can derive some lower limits on the spectral resolution by using simple estimates of the point spread function (PSF). The effective spectral resolving power of the G800L grism is the PSF of HST/ACS convolved with the intrinsic spectral resolving power of the grism. Using simulations with Tiny Tim one can estimate the PSF at the approximate wavelength of the Hα line. A Gaussian fit to the PSF simulations gives about 1.8±0.1 pixel (FWHM). Using an average dispersion of 40 Å/pixel this translates into a spectral resolving power of approximately 72 Å (FWFM) or R≈90 @ 6500 Å. However, a Gaussian fit to the cross-dispersion profile of a point-source spectrum gives values of roughly 2.1 pixel (FWHM), indicating that the grism mode of the ACS does not fully utilize the native spatial resolution of the direct imaging mode. The width of the effective PSF translates into a spectral resolving power of 84 Å (FWFM) or R≈77 @ 6500 Å.

In order to measure the spectral resolving power from the standard star spectra we used as template star a model spectrum of G191B2B taken from the HST CALSPEC library (g191b2b_mod_003.fits) and assumed it to be of essentially infinite resolution with respect to the observed spectrum. With IDL routines, the model spectrum and the observed spectra were re-binned to a common log normal wavelength step (1620 km/s per pixel). The amount of (Gaussian) broadening necessary to match the observed spectrum was then determined with the IDL routine ppxf (Cappellari & Emsellem, 2004).

The measurements for 20 individual exposures of the standard star give a median resolving power of R=66 @ 6563 Å corresponding to a FWHM of 100 Å. The results are shown in Figure 8 as function of spatial position. The mean statistical one-sigma error on an individual measurement is ±8 Å while the standard deviation of all 20 observations is 20 Å. Looking at Figure 8 it seems that there are potentially spectral resolving power variations with spatial position. For example, there appears to be a trend with the X-axis position with extreme values of 140 Å at small X-positions for CHIP 1. However, the field coverage is too sparse to draw any firm conclusions. Therefore, we conclude that the G800L grism in the WFC has a mean resolving power of 100±20 Å (FWHM) at 6563 Å. Comparing this value with the expectations from the spatial PSF only (i.e. 72 Å FWHM) shows that the grism itself contributes significantly to the broadening of the line spread function.

[1] By using stars of different spectral type with strong absorption lines at different wavelength one can potentially derive the spectral resolution as function of wavelength. It remains to be explored if this can be achieved with already existing observations from the archive such as parallel observations at low Galactic latitude.

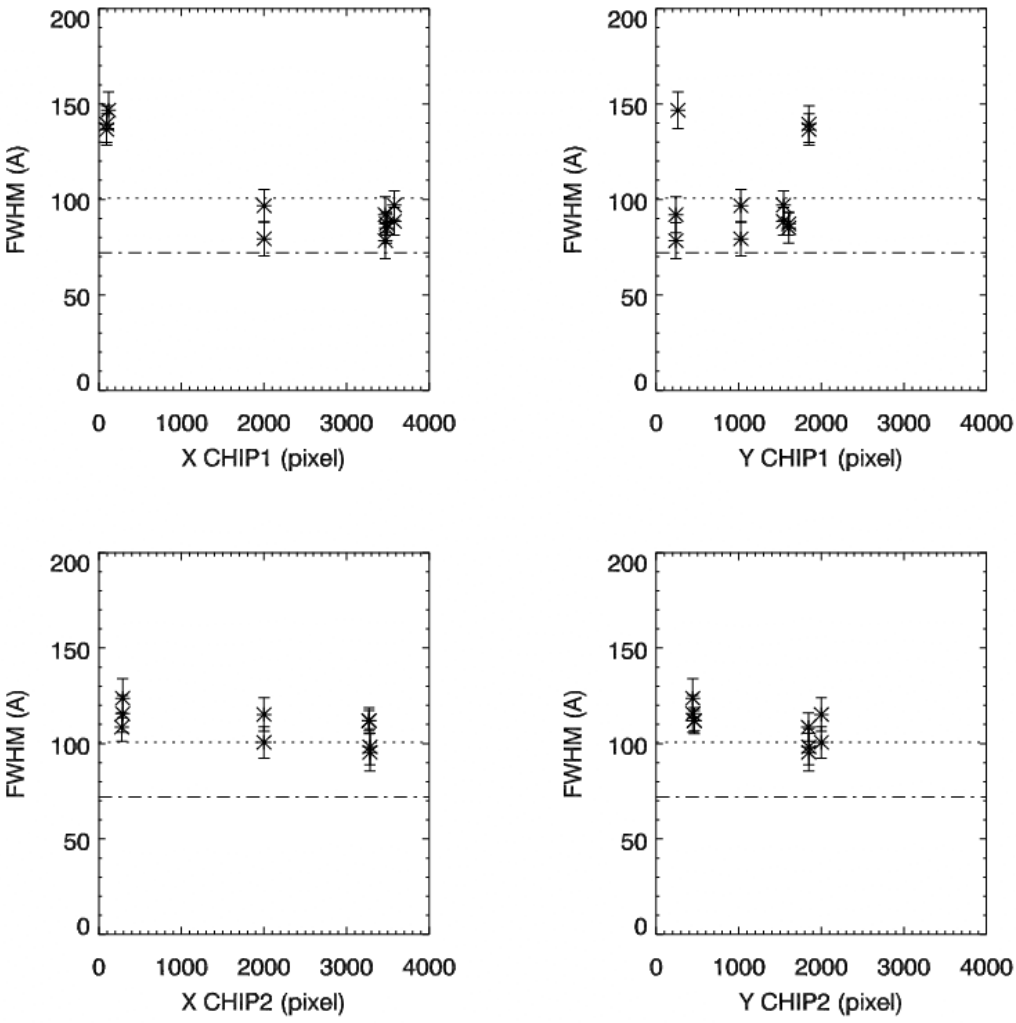

Figure 8: Spectral resolving power (FWHM in Å) as determined from the Hα line of the standard star G191B2B for 20 different exposures at various spatial positions. The dotted line shows the median value. The long dash-dotted line shows the expected spectral resolving power if only the HST/ACS point spread function is taken into account (see text for details).

7. Fringing properties

For the determination of sensitivity calibrations the standard star spectra must be extracted with the highest accuracy possible. The effect of fringing, which occurs due to the interference of incoming and reflected light within the detection layer of the CCD, can modulate the signal of the incoming light by large amounts in the

case of monochromatic light (±12% for the WFC). In this section we investigate if fringing for normal ACS/WFC spectroscopy is an important factor.

Knowing the construction of the CCD, the resulting fringe amplitude for the light falling on each CCD pixel can be computed using geometrical optics. Following the methods outlined in ST-ECF ISR 2003-03 (Walsh et al. 2003) we have developed the software to determine the fringing amplitude for any given CCD pixel. Starting from around 7000 Å, the characteristic fringing amplitude for the ACS CCD's steadily grows towards longer wavelengths. Due to the overlap with the second order and the significant drop in sensitivity (see Fig. 5) of the WFC CCD's, the measurement errors increase rapidly beyond 9500 Å. Approximately at this wavelength fringing has the largest impact on the extracted spectra (see also Walsh et al. 2003, Fig. 2).

Besides the CCD structure, which has been determined in Walsh et al. 2003 for both CCD's of the ACS, an important input for the fringe calculation is the form of the throughput function for the CCD pixels. We define the pixel throughput function as the relative distribution of light as a function of wavelength falling onto a given CCD pixel. In general this is the convolution of the intrinsic source spectrum with the line spread function (LSF) of the instrument. The determination of the throughput function and the computation of the fringing amplitudes would thus require the a priori knowledge of the source spectrum, which in general is not available.

However for continuum sources and the theoretical case of pure emission line objects[2], the throughput function can be estimated. For continuum sources the LSF dominates the form of the throughput function everywhere and the influence of the slowly varying source spectra can be neglected. For pure emission line sources the throughput function is solely determined by the intrinsic object spectrum. In what follows we estimate the fringing for these two extreme object classes.

Continuum sources: Our measurements in the previous section indicate that a realistic LSF (and therefore throughput function for fringing calculations) should have a near-Gaussian form with 100 Å FWHM at 6563Å. The LSF at 9500 Å, where the fringing amplitude has the largest impact on the extracted spectra, is expected to be slightly larger since the spatial PSF degrades towards larger wavelengths**.** However, we use here the value of 100 Å FWHM, which will slightly overestimate the fringing effects.

In order to investigate the magnitude of fringing for continuum sources, we computed the fringing amplitude of all pixels on both WFC CCD's at 9500 Å using

[2] As pure emission line sources we define objects with spectra composed of only isolated emission lines with internal line broadening << one pixel.

a Gaussian throughput function with 100 Å (FWHM). The effective minimum and maximum fringing amplitude is calculated as 0.999 and 1.001, respectively. We conclude that after using realistic values for the spectral resolving power and therefore pixel throughput functions, only negligible fringing (~0.1%) is expected at 9500 Å for continuum sources.

Using our Gaussian throughput function at all wavelengths we have analyzed the effect of fringing on extracted spectra by making a standard extraction of simulated continuum spectra of point-like objects with and without applying the fringing corrections. Figure 9 shows the quotient of these spectra for a selection of objects. In each panel, the chip number and the pixel position give the location of the spectrum.

It is evident from Fig. 9, that fringing is negligible (<0.1%) compared to the overall measurement errors for wavelengths up to 10000 Å. Beyond 10000 Å the contribution of fringing for continuum sources still remains small and not detectable, since the overall measurement errors increase due to a steep decline in system throughput.

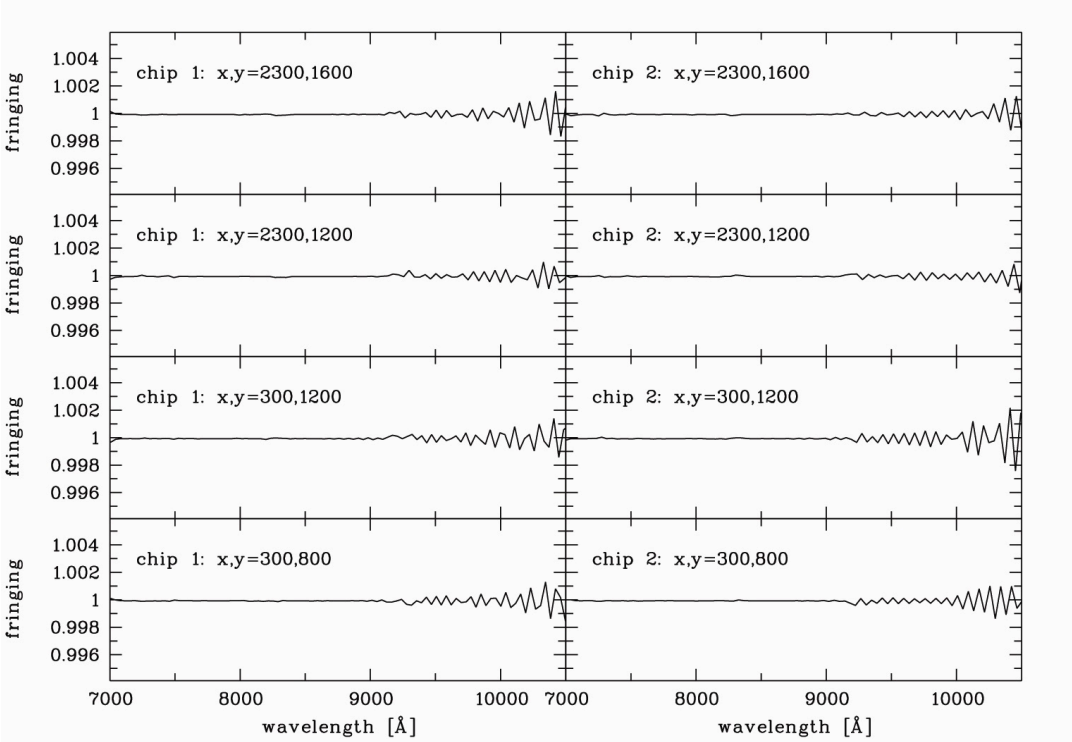

Figure 9: The effect of fringing determined by dividing the spectrum without fringe amplitudes applied with the spectrum to which calculated fringe amplitudes were applied to the CCD pixels before the extraction. The panels address various point-like objects at different positions across both CCD chips.

To measure the influence of the throughput function width on the fringing amplitude we have repeated the analysis presented in Fig. 9 using fringing determinations with Gaussian throughput functions of 20, 40, 60 and 80 Å FWHM width. The typical fringing errors at 9500 Å result in 5.0, 3.0, 1.0 and 0.3%, respectively. The main reason for the negligible fringing effects on the extracted spectra of continuum sources is indeed the smoothing effect of the rather large LSF of approximately 100 Å (FWHM) of the G800L grism.

Pure emission line source: For these objects the throughput function for the CCD pixels is entirely determined by the width of the intrinsic source spectrum, for which no general lower limit can be given. Smaller throughput functions cause larger amplitudes for the fringing, and technically it would be possible to use our fringing model with Gaussian throughput functions of 0.2 Å (FWHM) and lower. On the other hand it might be dangerous to stress the model by using throughput functions smaller than 20 Å (FWHM), which was the width of the monochromator observations on which it is based. As a compromise we use the monochromator data taken with 20Å (width) throughput function to estimate a *lower limit* for the effect of fringing on pure emission line sources.

As can be verified in Walsh et al. (2003), Fig. 11, typical fringing amplitudes in the data taken at 9440 Å are 12%. The size of minima and maxima in the fringing amplitude is roughly equal to the size of the instrumental LSF and PSF, which determine the extent of pure emission line sources in dispersion and spatial direction, respectively. Thus fringing can, in the idealized case of a pure emission line, cause variations in line flux of 12% and more.

In practice the effects of fringing are less dramatic. For example, in the emission line spectrum of a Wolf-Rayet star (Programme 10058) we measured line flux variations of 5% between 13 individual observations at a wavelength of 9700 Å. Comparison with a continuum region of the same star revealed that 2% variation can be accounted for by flat-fielding and sensitivity calibration errors. We conclude that fringing for emission lines seen in a WR star causes variations of about 4%.

8. Conclusions

This ISR presented an up-dated flux calibration for the ACS/WFC G800L data using the revised wavelength calibrations of Larsen et al. 2005. The first order of the grism in conjunction with the aXe reduction software provides an absolute flux calibration to better than 2% for the spatial positions covered in this ISR. The new sensitivity files for the first order and other orders are provided via the ST-ECF WEB pages. We also measured the spectral resolving power from the Hα

absorption line of the flux standard star G191B2B yielding an effective FWHM of 100±20 Å.

We further demonstrate that the effect of fringing in the extraction of slitless spectra from WFC slitless images can be neglected (variations <0.1%) for continuum sources such as the white dwarfs used for the flux calibration. An identical analysis for the slitless mode of the HRC channel with the G800L grism provides similar conclusions. For extreme objects, such as pure emission line sources, fringing can introduce significant variations (12% and more) in the measured flux between different positions. However, for more typical emission line objects, such as WR stars, we detect an error in the measured emission line fluxes of only ~4% over and above flux and flat-field calibration errors of 2%.

Acknowledgements

We thank Wolfram Freudling, Ralph Bohlin and Ron Gilliland for helpful comments on this ISR.

References

Cappellari M., Emsellem E., 2004, PASP, 116, 138

Kümmel, M., Larsen, S.S., & Walsh, J.R.: "Slitless Spectroscopy with the Advanced Camera for Surveys", 2006, The 2005 HST Calibration Workshop, STScI

Larsen, S.S., Walsh, J.R.: "Updated Wavelength Calibration for the WFC/G800L grism", 2005, ST-ECF ISR ACS 2005-08

Walsh J.R., Freudling W., Pirzkal N. & Pasquali A.,: "Modelling the fringing of the ACS WFC and HRC chips", 2003, ST-ECF ISR ACS 2003-03

Appendix A

Table 1: Log of calibration exposures used in this ISR.

Filename	Targer	Proposal ID	FILTER1	EXPTIME (sec)	POSTARG1 (arcsec)	POSTARG2 (arcsec)
j8ca06hzq_flt.fits	GD153	9029	F775W	2	64.68	-24.62
j8ca06i0q_flt.fits	GD153	9029	G800L	60	64.68	-24.62
j8caa5vvq_flt.fits	GD153	9029	F775W	2	71.67	34.07
j8caa5vwq_flt.fits	GD153	9029	G800L	60	71.67	34.07
j8caa5vxq_flt.fits	GD153	9029	G800L	60	71.67	34.07
j8cab5vyq_flt.fits	GD153	9029	F775W	2	64.68	-24.62
j8cab5w0q_flt.fits	GD153	9029	G800L	60	64.68	-24.62
j8eu04aeq_flt.fits	G191B2B	9568	F775W	1	-91.16	30.39
j8eu04afq_flt.fits	G191B2B	9568	G800L	15	-91.16	30.39
j8eu04agq_flt.fits	G191B2B	9568	F775W	1	-91.16	30.39
j8eu04ahq_flt.fits	G191B2B	9568	G800L	15	-91.16	30.39
j8eu04ajq_flt.fits	G191B2B	9568	F775W	1	-91.16	-45.50
j8eu04akq_flt.fits	G191B2B	9568	G800L	15	-91.16	-45.50
j8eu04amq_flt.fits	G191B2B	9568	F775W	1	0.00	0.00
j8eu04anq_flt.fits	G191B2B	9568	G800L	15	0.00	0.00
j8eu04aoq_flt.fits	G191B2B	9568	F775W	1	0.00	0.00
j8eu04apq_flt.fits	G191B2B	9568	G800L	15	0.00	0.00
j8eu05b5q_flt.fits	G191B2B	9568	F775W	1	-83.67	34.00
j8eu05b6q_flt.fits	G191B2B	9568	G800L	15	-83.67	34.00
j8eu05b8q_flt.fits	G191B2B	9568	F775W	1	-83.67	-35.43
j8eu05b9q_flt.fits	G191B2B	9568	G800L	15	-83.67	-35.43
j8eu05baq_flt.fits	G191B2B	9568	F775W	1	-83.67	-35.43
j8eu05bbq_flt.fits	G191B2B	9568	G800L	15	-83.67	-35.43
j8eu05bgq_flt.fits	G191B2B	9568	F775W	1	0.15	48.42
j8eu05bhq_flt.fits	G191B2B	9568	G800L	15	0.15	48.42
j8eu05biq_flt.fits	G191B2B	9568	F775W	1	0.15	48.42
j8eu05bjq_flt.fits	G191B2B	9568	G800L	15	0.15	48.42
j8eua4asq_flt.fits	G191B2B	9568	F775W	1	71.67	34.07
j8eua4atq_flt.fits	G191B2B	9568	G800L	15	71.67	34.07
j8eua4auq_flt.fits	G191B2B	9568	F775W	1	71.67	34.07
j8eua4avq_flt.fits	G191B2B	9568	G800L	15	71.67	34.07
j8eua4azq_flt.fits	G191B2B	9568	F775W	1	71.67	-33.03
j8eua4b0q_flt.fits	G191B2B	9568	G800L	15	71.67	-33.03
j8eua4b1q_flt.fits	G191B2B	9568	F775W	1	71.67	-33.03
j8eua4b2q_flt.fits	G191B2B	9568	G800L	15	71.67	-33.03
j8eua5bmq_flt.fits	G191B2B	9568	F775W	1	64.68	45.36
j8eua5bnq_flt.fits	G191B2B	9568	G800L	15	64.68	45.36
j8eua5boq_flt.fits	G191B2B	9568	F775W	1	64.68	45.36

j8eua5bpq_flt.fits	G191B2B	9568	G800L	15	64.68	45.36
j8eua5buq_flt.fits	G191B2B	9568	F775W	1	64.68	-24.62
j8eua5bvq_flt.fits	G191B2B	9568	G800L	15	64.68	-24.62
j8eua5bwq_flt.fits	G191B2B	9568	F775W	1	64.68	-24.62
j8eua5bxq_flt.fits	G191B2B	9568	G800L	15	64.68	-24.62
j97e04rpq_flt.fits	G191B2B	10374	G800L	27	0.00	0.00
j97e04rqq_flt.fits	G191B2B	10374	G800L	27	0.00	0.00
j97e04rtq_flt.fits	G191B2B	10374	F775W	1	0.00	0.00
j97e04ruq_flt.fits	G191B2B	10374	F775W	1	0.00	0.00

Appendix B

Table 2: Flux versus extraction aperture half-width for the G800L grism in the WFC (1st order), relative to the default aperture half-width of 0.5 arcsec. The corrections are listed for five different wavelength ranges. An electronic version of this table can be obtained from http://www.stecf.org/instruments/ACSgrism.

Half-width (pixels)	Half-width (arcsec)	Flux/Flux(0.5") [550-650 nm]	Flux/Flux(0.5") [650-750 nm]	Flux/Flux(0.5") [750-850 nm]	Flux/Flux(0.5") [850-950 nm]	Flux/Flux(0.5") [950-1050 nm]
2	0.100	0.825	0.814	0.793	0.750	0.637
3	0.150	0.912	0.907	0.896	0.865	0.765
4	0.200	0.946	0.943	0.937	0.920	0.839
5	0.250	0.965	0.962	0.958	0.946	0.883
6	0.300	0.978	0.976	0.972	0.963	0.917
8	0.400	0.991	0.991	0.991	0.987	0.964
10	0.500	1.000	1.000	1.000	1.000	1.000
12	0.600	1.006	1.006	1.007	1.009	1.027
14	0.700	1.011	1.011	1.012	1.015	1.047
16	0.800	1.015	1.015	1.017	1.021	1.066
18	0.900	1.017	1.018	1.020	1.025	1.080
20	1.000	1.019	1.020	1.023	1.028	1.094
22	1.100	1.021	1.022	1.025	1.031	1.105
24	1.200	1.023	1.023	1.027	1.034	1.115
26	1.300	1.025	1.025	1.029	1.036	1.120
28	1.400	1.026	1.026	1.030	1.038	1.128
30	1.500	1.028	1.027	1.031	1.039	1.136
35	1.750	1.031	1.031	1.034	1.042	1.150
40	2.000	1.034	1.033	1.037	1.045	1.160